

# ArtA: Automating Design Space Exploration of Spin Qubit Architectures

Nikiforos Paraskevopoulos<sup>1,2</sup>, David Hamel<sup>1</sup>, Aritra Sarkar<sup>1,2</sup>, C. G. Almudever<sup>3</sup>, and Sebastian Feld<sup>1,2</sup>

<sup>1</sup>Quantum and Computer Engineering Department, Delft University of Technology, 2628 CD Delft, The Netherlands

<sup>2</sup>QuTech, Delft University of Technology, 2628 CJ Delft, The Netherlands and

<sup>3</sup>Computer Engineering Department, Universitat Politècnica de València, Camino de Vera, s/n, 46022 València, Spain

In the fast-paced field of quantum computing, identifying the architectural characteristics that will enable quantum processors to achieve high performance across a diverse range of quantum algorithms continues to pose a significant challenge. Given the extensive and costly nature of experimentally testing different designs, this paper introduces the first Design Space Exploration (DSE) for quantum-dot spin-qubit architectures. Utilizing the upgraded SpinQ compilation framework, this study explores a substantial design space comprising 29,312 spin-qubit-based architectures and applies an innovative optimization tool, ArtA (Artificial Architect), to speed up the design space traversal. ArtA can leverage seventeen optimization method configurations, significantly reducing exploration times by up to 99.1% compared to a traditional brute force approach while maintaining the same result quality. After a comprehensive evaluation of best-matching optimization configurations per quantum circuit, ArtA suggests universal architectural features that perform optimally across all examined circuits, emphasizing the importance of maximizing quantum gate parallelization at the expense of more crosstalk interference.

## I. INTRODUCTION

As the field of quantum computing rapidly advances, different qubit technologies exhibit unique hardware and performance characteristics. It still remains to be seen which one (e.g., superconducting, trapped ions, quantum dots, photonics, defect-based on nitrogen-vacancy diamond centers) will succeed in scaling up quantum computing systems with high-quality qubits [10, 54]. Among them, spin qubits in quantum dots emerge as a compelling avenue for achieving scalability for practical quantum computation [10]. To this day, spin qubits are at an early stage in their development, with Intel's Tunnel Falls chip currently boasting the highest count of twelve spin qubits [31]. Despite this, their inherent scalability advantages suggest that a robust two-dimensional design [6, 35, 62] could be scaled up relatively easily once fabrication techniques and quality improve up to a certain level. Designing a chip, however, involves multiple architectural design choices whose impact in the future can only be fully assessed through experimental studies post-scaling the technology. Exploring all these design possibilities simultaneously can be expensive, time-intensive, and impractical. Therefore, simulating how different design choices can affect performance in a range of quantum applications is crucial to assist the development. This process facilitates highlighting architectural insights that can guide the technology forward and will allow quantum researchers to make more informed decisions, streamline efforts, and hasten the development of these devices.

Recognizing the intricate challenges of designing quantum processor architectures, this study initiates the first Design Space Exploration (DSE) for spin-qubit architectures, both from a current technological perspective and a future one. Therefore, in this work, we have identified a wide range of representative architectural features and abstracted them into usable input variables, resulting in 29,312 different architectures. To facilitate this exploration, we have enhanced the compilation capabilities of SpinQ compilation framework [46] to handle all these input variables and updated the def-

inition of the Estimated Success Probability (ESP) metric to include not only operational errors but also crosstalk and decoherence errors. These transformations and many more establish SpinQ as the first compilation and DSE framework for spin qubit architectures.

DSE processes [38, 49], which rely on a brute force approach to traverse and subsequently analyze the design space, will be impractical time-wise, especially for such large spaces. Our approach, however, employs ArtA (*Artificial Architect*), a built-in tool containing multiple optimization methods designed to automate the DSE process of SpinQ, thus taking less time than the brute force approach with the same quality of results. The abilities of ArtA are (a) to suggest which of the seventeen optimization configurations can find the architecture with the desired ESP the fastest compared to the brute-force approach and (b) which architectural design characteristics are key for building high-performance spin-qubit devices per quantum benchmark circuit.

Our results demonstrate ArtA's ability to compare all optimization techniques for each quantum circuit and obtain a solution up to 99.1% faster, on average, than brute-forcing. Then, equipped with these insights, we move on to conduct a DSE analysis of 29,312 spin qubit architectures and provide valuable insights into best design practices. Firstly, we highlight the critical need to maximize the parallelization of quantum gates rather than minimizing crosstalk between qubits. Secondly, we find that the communication method with shuttle operations is better in large-scale circuits than SWAPs, but for single-qubit gates, pulse-based methods rotations are preferred over shuttle-based. Finally, our universal architecture for all used quantum circuits suggests that the likelihood of success increases when prioritizing the parallelization of single-qubit gates instead of two-qubit gates.

The main contributions of this paper:

1. The design space definition comprising of abstracted characteristics of current and, potentially, future spin qubit architectures.
2. The new SpinQ, the first compiler and DSE framework

for spin qubit architectures. In this version, we have updated the ESP formula to include operational, crosstalk, and decoherence-induced errors.

3. ArtA, the first tool consisting of seventeen optimization method configurations automating the DSE process of spin qubit architectures.
4. Evaluation of best-matching optimization configurations per quantum circuit.
5. Evaluation of best-matching architectural characteristics per quantum circuit and universally (i.e., for all used circuits) in terms of ESP.

The remainder of this paper is structured as follows: In Section II, we discuss the scalability potential of quantum-dot spin qubits as well as the importance of addressing engineering challenges while taking into account the resulting performance of the final architecture. Then, in Section III, we motivate the need for an automated Design Space Exploration analysis for spin qubit devices and formulate four research questions for this work. After that, in Section IV, we define the design space consisting of various input architectural variables and establish the new DSE functionality of SpinQ. Another upgrade in SpinQ is the enhanced Estimated Success Probability metric, described in Section V, which is used as the Figure of Merit for our exploration. In Section VI, we introduce ArtA (Artificial Architect) and two new metrics to evaluate its performance. In the results Section VII, we first evaluate ArtA’s performance across all used quantum circuits and determine the best optimization method configuration. Then, we conduct a detailed analysis of the best architectural designs for each quantum circuit and form valuable insights for a universal architecture. We conclude our work and provide ideas for future directions in Section IX.

## II. CHALLENGES FOR SCALING UP SPIN QUBIT DEVICES

Spin-qubit technologies are distinguished by their unique physical features, which position them as a highly scalable solution for quantum computing. The advantages of spin-qubits include a significantly smaller size — up to a thousand times less than other qubit technologies — combined with decades of semiconductor manufacturing expertise, long coherence times coupled with short gate durations, and high temperatures [9, 10, 29, 37, 62, 65, 67, 70, 71, 73]. At the core is the quantum dot, which contains a trapped electron(s) or hole(s) to form a physical qubit [25]. Spin qubits are manipulated electromagnetically using multiple precision-engineered gate electrodes that facilitate either single- or two-qubit operations through exact timing of pulse sequences across various quantum dot configurations. Recent studies have expanded these systems into one-dimensional and two-dimensional arrays [5, 29], exploring different structures and material combinations.

Despite the mentioned advantages, spin qubit quantum processors are not as advanced as other qubit technologies in

terms of qubit counts and availability. Major technological hurdles are related to the so-called interconnect bottleneck [62], and various fabrication challenges towards scaling up [4, 8, 16, 17]. On the upside, there have been significant efforts [7, 20, 30, 35, 44, 47, 62, 64] to tackle these challenges.

However, solving them can not guarantee successful quantum algorithm executions. This is because the quality and quantity of qubits are not the only factors determining a high-performing quantum processor. The architectural constraints qubits need to comply with are equally important in *how* they are operated. For instance, the benefits of qubits with excellent operational fidelity can easily be outweighed by low qubit connectivity and limited natively supported quantum gates. Similarly, high-quality qubits with low crosstalk interference are not enough when they can not be addressed in parallel. These, and many more, are interlinked architectural trade-offs that affect the actual performance of the quantum processors.

During the Noisy Intermediate-Scale Quantum (NISQ) era [50], predicting which architectural features and trade-offs will facilitate successful quantum circuit executions while maintaining reasonable hardware requirements remains challenging. To date, there has not been a systematic study exploring spin-qubit architectures through this prism of providing concrete guidelines for future development. Therefore, in this study, we exploit such an opportunity and alleviate the need for time-consuming, expensive, and technology-dependent experimental studies.

## III. PROBLEM STATEMENT

The need to apply design space exploration (DSE) techniques for designing and optimizing full-stack quantum computing systems, or components thereof, has been emphasized in previous work [1]. These techniques have been successfully applied across different levels of the quantum computing stack. For instance, DSE has been used to explore ion-trap quantum processors [40] and evaluate compilation techniques for superconducting qubits [53]. Such techniques can abstractly convert architectural characteristics into design variables and, in this way, quantize the design space, expressing current and future design possibilities that otherwise would be impossible or too time-consuming to physically realize. Starting from there [38, 49], the steps for a proper DSE: i) Describe the problem in terms of input variables or parameters (design choices), ii) select the performance metrics, iii) choose a global cost function as a Figure of Merit that combines different performance metrics, and iv) find models (behavioral, analytical, experimental data) that connect input parameters with metrics (or directly to the Figure of Merit). By using these DSE techniques, performance trends can be observed projecting current or future multidimensional design spaces, and points of optimality can be identified. From such an approach, it can be determined which architectural design choices (i.e., combinations of input parameter values) could provide better performance when benchmarked from small to large-scale quantum circuits.

Although this methodology is well established and under-

stood in many disciplines, it can be challenging to implement in such early stages for spin-qubit technologies. One of the most difficult aspects is the development of a simulation framework incorporating a range of representative architectural variables adopting a large-scale perspective. Firstly, it is difficult to predict which architectural features will be relevant for many generations of devices to come, and secondly, the framework itself has to be flexible to incorporate new ones easily.

In practice, this can be very time-consuming, and thus, typically, the design space is kept at a reasonable and, usually, small scope under specific technological assumptions. Considering the rapid progress of spin-qubits, the potential design space can be enlarged quickly with new considerations, rendering any previous exploration obsolete. Hypothesizing such a conventional DSE framework exists, it can be tedious to brute force thousands of designs and extensively analyze results. Hence, the relevancy of a framework automating such a DSE process, which can simplify performance evaluation of different spin-qubit architectures, is prominent.

To capture the above problem statement, we ask the following four research questions:

1. What characteristics of spin-qubit architectures are representative, and how can they be incorporated in a DSE framework? Answered in Section IV
2. How can a DSE framework for investigating preferred spin-qubit architectural characteristics be constructed? Answered in Section IV
3. Which optimization methods are best suited for automating the DSE? Answered in Section VII A
4. Which architectural characteristics in the selected design space are key for building high-performance spin-qubit devices for specifically given quantum circuits? Answered in Section VII B

#### IV. SPINQ AND THE DESIGN SPACE

To answer the first two research questions, we conducted an analysis of relevant spin-qubit architectural properties with a long-term view and distilled them into numerous variables. These properties were selected to be representative of spin qubit devices as well as to create trade-offs between them. The latter will prevent maximizing one without causing a performance penalty through another (refer to Section V). The defined design space is summarized in Table I, including their possible values. It should be noted that the DSE analysis in this work uses either discrete or categorical variables [41], as we aim to provide performance trends and rankings between optimization algorithms and architectures rather than absolute comparisons. An architecture is then characterized by one (valid) combination of variable values. Below, we describe the considered design space.

TABLE I: Summary of values of the considered architecture variables.

Variable	Values	
<b>xy_z</b>	0 → No parallelization 1 → Parallelization	
<b>xy_tqg</b>	idem	
<b>z_tqg</b>	idem	
<b>xy_z_tqg</b>	idem	
<b>xyD</b>	-1 → Non applicable 1 → No parallelization 25 → 25% of total qubits parallelization for X/Y gates 50 → idem, 75 → idem, 100 → idem	Sec. IV.A
<b>zD</b>	idem	
<b>tqgD</b>	1 → no parallelization 25 → 25% of total qubits/2 parallelization for two-qubit gates 50 → idem, 75 → idem, 100 → idem	
<b>sID</b>	1 → No parallelization 25 → 25% of total qubits parallelization for shuttles 50 → idem, 75 → idem, 100 → idem	
<b>single_qubit_impl</b>	0 → Sequential 1 → Local 2 → Global 3 → Semi-global	
<b>z_rot_impl</b>	0 → Shuttle-based 1 → Pulse-based	Sec. IV.B
<b>Router</b>	0 → Shuttle-based SWAP router 1 → beSnake router	Sec. IV.C
<b>degree</b>	4 → Square connectivity 6 → One extra diagonal 8 → Two extra diagonals	Sec. IV.D
<b>SWAP_opt</b>	0 → SWAP replacement used 1 → SWAP replacement is not used	Sec. IV.E

##### A. Operational gate constraints

The set of gate constraints can be vast; therefore, we decided to abstract them into the following variables that affect which (a) gate types (i.e., executed simultaneously) and (b) how many of them can be parallelized at the same time step. To highlight an example of a design trade-off, we note that the higher the degree of parallelization, the shorter the circuit depth will be, and therefore, the shorter the algorithm execution time, but it will result in higher crosstalk.

##### a) Combinations of gate types that can be parallelized:

$$(xy\_z, xy\_tqg, z\_tqg, xy\_z\_tqg = 0, 1)$$

As the names suggest, these variables are boolean and signify whether specific gate types can be executed in parallel. For example,  $xy\_z$  defines if X/Y can be executed simultaneously with Z gates.

##### b) Constraints affecting the parallelization per gate

### type expressed in percentage:

( $xyD, zD, tqgD, sD = -1, 1, 25\%, 50\%, 75\%, 100\%$ )

These variables indicate how many gates, for each type, can be parallelized, expressed as a percentage relation to the total number of qubits. For example,  $xyD = 25$  in a 40-qubit architecture means that at most ten X or Y gates can exist in a single cycle. Note that the notion of a cycle refers to the basic unit of time representing one step in a sequence of gates of a quantum circuit, and each step may contain multiple gates. The  $zD$  and  $sD$  variables indicate the same for Z rotations and shuttle gates, respectively. The  $tqgD$  variable indicates the parallelization amount for two-qubit gates. As these always involve two qubits, they are expressed as a percentage of half of the total number of qubits. A value of  $-1$  means that the parallelization degree is not user-defined but dictated by a specific single-qubit gate implementation explained next.

### c) Single-qubit gate implementation:

( $single\_qubit\_impl = 0 \rightarrow Sequential, 1 \rightarrow Local, 2 \rightarrow Global, 3 \rightarrow Semi-global$ )

This variable indicates in what manner single-qubit gates are carried out. A *Global* single-qubit gate implementation means the same rotation axis and angle are applied to all qubits. For qubits that do not participate in a cycle, locally applied disable instructions prevent their rotation. Then, the *Semi-Global* implementation is considered with the same rotation scheme as in [27] and [46], which is essentially equivalent to the implementations of the crossbar architecture proposed of [35]. In this implementation, qubit rotations are implemented semi-globally, meaning that either all qubits in odd or even column parities can be rotated at a time with the same axis and angle, and unwanted qubit rotations have to be reversed afterward by additional instructions [46]. A *Local* single-qubit gate implementation allows for any parallelized combination of gates at any angle to be executed in a cycle. Finally, a *Sequential* single-qubit gate implementation does not allow any gate parallelization, meaning that every cycle will be occupied by one gate only. It should be noted that depending on the  $single\_qubit\_impl$  value, only certain combinations of categories (a) and (b) are possible. For instance, in the *Global* and *Semi-Global* implementations, the  $xyD$  variable is not applicable as these implementations predetermine the upper limit of single-qubit gates allowed during a cycle.

### B. Implementation of Z rotations:

( $z\_rot\_impl = 0, 1$ )

This boolean variable also stipulates the implementation of Z rotation gates on a hardware level. The first option is a high-fidelity shuttle-based Z rotation, which is achieved

with two time-sensitive qubit shuttles to and from a neighboring column [27, 35, 39, 46]. This single-qubit manipulation belongs to the so-called “hopping spins” type [66], and it is possible to achieve an arbitrary rotation axis, but in this work, we assume the aforementioned implementation proposal for simplicity. The second option is a regular pulse-based Z rotation, where Z gates are implemented similarly to X/Y gates by applying pulses. With the first choice being a unique characteristic of spin-qubits, we are interested in exploring which one of the two provides better performance across many quantum circuits. Similarly to the variables mentioned earlier, only certain combinations are possible depending on  $single\_qubit\_impl$  values. For example, with a *Semi-Global* single-qubit gate implementation and a pulse-based Z rotation gate, the  $zD$  variable is not applicable for the same reason the  $xyD$  variable is not applicable, as we explained before in category (b).

### C. Connectivity of the device:

( $degree = 4, 6, 8$ )

This variable stipulates the considered coupling graphs by addressing them through their average node degree. A coupling graph is a graph of possible direct interactions (edges) between qubits (nodes). The first coupling graph we used is a square grid ( $degree = 4$ ). The second is identical to the first but adds one diagonal connection in each square (i.e., each qubit is coupled with six neighboring qubits and with three at the corners,  $degree = 6$ ). Finally, the third adds the second diagonal in each square (i.e., each qubit is coupled with eight neighboring qubits and with three at the corners,  $degree = 8$ ). Figure 1, presents the coupling graphs considered with color-coded edges for each of the three types. We have now reviewed all the variables related purely to hardware. Next, we will consider two variables associated also with the compilation process. More specifically, they change the routing process based on the hardware communication constraints.

### D. Routing methods:

( $router = 0 \rightarrow Shuttle-based SWAP, 1 \rightarrow beSnake$ )

There are two routing algorithm choices. The first one, introduced in [39, 46], is a *shuttle-based SWAP* routing algorithm. In particular, this algorithm was tailored around the unique constraints of the crossbar architecture [35], which necessitated the maintenance of the checkerboard physical qubit pattern to achieve a time-efficient compilation process. One of the advantages of this algorithm is, in fact, the maintenance of the checkerboard pattern, which in turn keeps the crosstalk effect low and enables the *Semi-Global* rotations scheme exclusively. The second routing option is called *beSnake* [45], and it is capable of freely shuttling qubits around any topology and in any direction, handling complex routing scenarios involving parallelized gates.

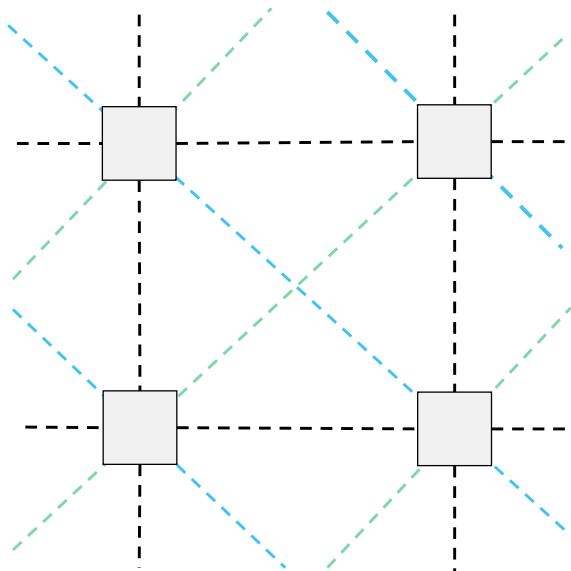


FIG. 1: The different coupling graphs considered in the design space. The coupling graph consists of the black lines and edges when  $\text{degree} = 4$ , black and green lines when  $\text{degree} = 6$ , and all lines when  $\text{degree} = 8$ .

### E. SWAP replacement:

( $\text{SWAP}_{\text{opt}} = 0, 1$ )

This binary variable concerns an optional functionality of the beSnake routing algorithm, which can replace a sequence of shuttles with a SWAP operation under certain conditions [45]. These conditions are satisfied when the accumulated fidelity of a parallelized shuttle sequence exceeds the fidelity of only executing a SWAP on that particular location. This variable is useful for creating insights for architectures that support SWAPs compared to others that do not support them.

### F. Design interdependencies and verification

All these variable values act as input into the upgraded SpinQ housing its new configurable compiler, making it the first compilation and DSE framework for spin-qubit architectures. After this upgrade, we are able to provide SpinQ with multiple combinations of variable values, compile each input circuit iteratively for all valid architectures, and calculate and store the same performance metrics used in [46]. These are gate overhead, circuit depth overhead, and Estimated Success Probability (ESP) of the compiled quantum circuit(s).

As mentioned, not all combinations of variable assignments are valid, as there are interdependencies between them; hence, SpinQ automatically filters the design space to allow only valid combinations. If all combinations were allowed, presented in Table I, there would be a total of 1, 105, 920 architectures, but the valid ones used in this work amount to 29, 312. Figure 2 shows the interdependencies tree that SpinQ uses to filter valid architectures.

Another significant component of SpinQ is the compiler

verification tool [46]. This tool is crucial, given the absence of real devices for testing. The verification functions have been enhanced to handle all valid architectures via our two-step method, which thoroughly scrutinizes circuits at each compilation stage [46].

## V. FIGURE OF MERIT

To estimate the performance of any quantum processor, a prevalent method when the device is not physically available is through the Estimated Success Probability (ESP) [42, 52] extracted from the compiled circuit. This approach is by far the most efficient compared to Schrodinger-Feynman, tensor networks, or noise model simulations as all become exponentially slower with larger circuits and/or higher qubit connections on the device [46]. The choice of the figure of merit is a crucial step to ensure fair results, as every design variable needs to be directly linked to the resulting value, along with their trade-offs. This will prevent ArtA (introduced later in Section VI) from maximizing some variable(s) and, by doing so, unfairly favoring specific architectures. For example, it will not be fair to be able to maximize the parallelization degree of all gates without causing some negative impact due to increased crosstalk. Such a consideration also expresses more accurately design decisions in real experimental quantum processors.

In this work, we start from the ESP definition of [46] given in Equation 1 and expand it to reflect all previous considerations, given in Equation 2, with now three components in total: a gate operations term, a crosstalk term, and a decoherence term.

$$ESP = \prod_k \prod_i F_{i,k} \quad (1)$$

where  $k$  represents the  $k$ th time step and  $i$  the  $i$ th gate in the  $k$ th time step.

$$ESP = \left( \prod_k \prod_i F_{i,k} \right) \cdot \left( \prod_k \prod_{i,j} C_{i,j,k} \right) \cdot (1 - e^{(-t/T_2)})^N \quad (2)$$

where  $k$  represents the  $k$ th time step,  $i$  the  $i$ th gate in the  $k$ th time step and  $j$  represents the  $j$ th gate that inflicts crosstalk with the  $i$ th gate.  $F$  is the fidelity and  $C$  the crosstalk of the corresponding gates. The last term, adapted from [27], introduces the decoherence-induced errors, which represent the probability of all qubits staying coherent during the execution of the circuit.  $T_2$  is the decoherence time,  $t$  the duration time of the circuit, and  $N$  the total number of qubits. We will discuss each of the terms in detail in the next three subsections.

### A. Gate operations term

The choice of typical operational fidelities of each gate, coined by the  $F_{i,k}$  term, plays a large role in the probability

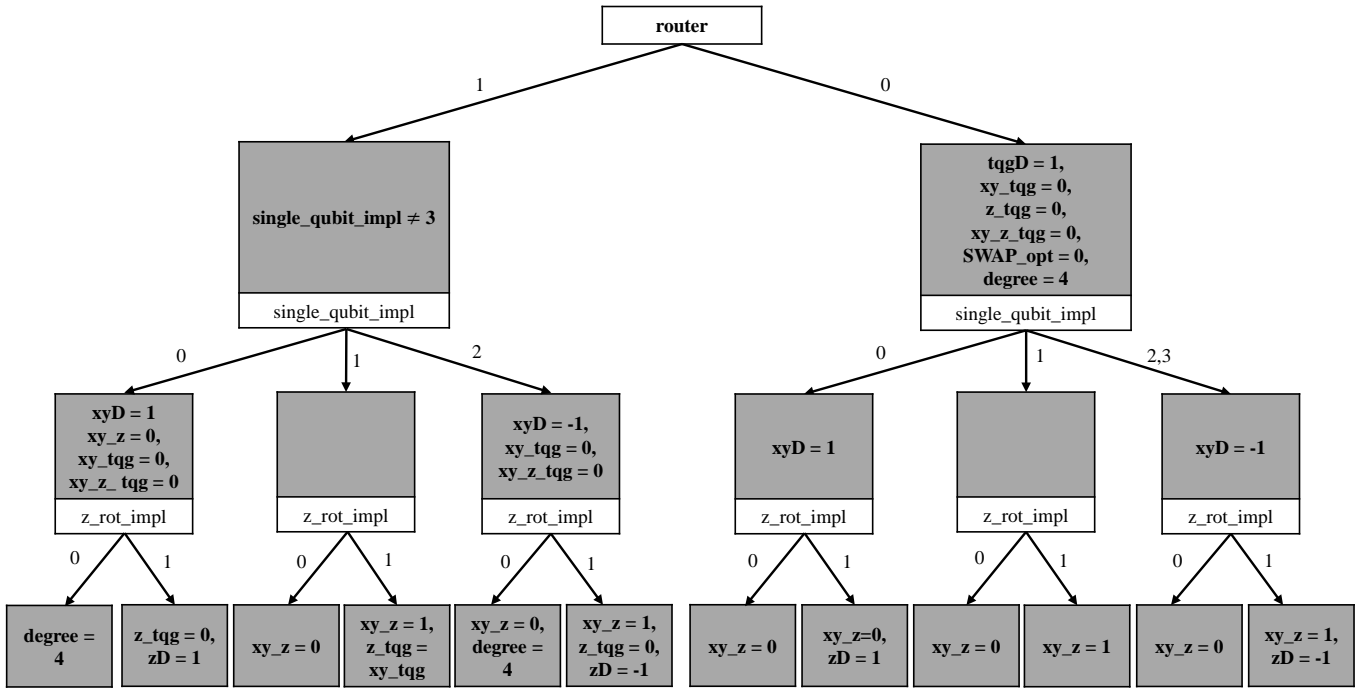


FIG. 2: Tree of valid architectural configurations that SpinQ can handle

of success of quantum circuits. In our analysis, we consider these fidelities to be constants within the design space rather than variables. This is because determining the optimal fidelity value for enhancing the ESP is straightforward; higher operational fidelity invariably leads to improved performance. Since we are conducting an exploration, we take a highly optimistic approach to the state-of-the-art [43, 48, 69] values for each gate type<sup>1</sup>:

$$F_{\text{single-qubit}} = 0.9999, F_{\text{two-qubit}} = 0.9998 \quad (3)$$

### B. Crosstalk term

Crosstalk has been sparsely studied for spin qubits. This is because the crosstalk effects when executing multiple gates in parallel in close proximity are still very complex to model accurately [26, 60]. Nonetheless, the presence of crosstalk is expected to have a large influence on quantum computer performance in the future, and current proposals are already suggesting techniques to mitigate it in simple forms [60]. For our purposes, crosstalk creates necessary trade-offs between architectural variables, and, as explained before, this is essential for a fair ESP calculation across architectures. For

these reasons, we have devised a model to help us discover relative categorical differences between architectures, rather than accurate predictions of crosstalk effects. Our overall aim is not to approximate the actual performance of designs but to pronounce their differences by creating a performance order between them. We further assume that crosstalk should depend on local hardware characteristics between any two nearest-neighboring qubits being operated at the same time, and since this information is already included in the operational fidelity of each gate type, our crosstalk definition is a function of those. Below, we summarize our assumptions:

- Nearest-neighbor crosstalk only (i.e., a pair of qubits that are directly connected by an edge in the coupling graph)
- Crosstalk occurs for each edge connecting qubits, which are operated in parallel by different gates
- There should be some correlation between the fidelity of gates and crosstalk effects, as they are both influenced by the same quality of fabrication
- The crosstalk occurring between neighboring qubits on which two different quantum gates are applied should not be higher than the combined operational error of these two gates

Based on these assumptions, we calculate the crosstalk effect as follows:

$$C_{i,j,k} = \left( \frac{2}{\frac{1}{F_{i,k}} + \frac{1}{F_{j,k}}} \right)^n \quad (4)$$

<sup>1</sup> Another reason we do so is to avoid *numeric underflows* where there is a loss of accuracy in numerical calculations if ESP becomes smaller than the smallest positive representable value in a programming language's floating-point arithmetic.

where  $n$  is the number of the total direct links (i.e., nearest-neighbors) on the topology between the  $i$ th and the  $j$ th operation. Similarly to before,  $F$  corresponds to the operational fidelity.

A schematic overview of crosstalk effects is given in Figure 3. We see two two-qubit gates acting within the red ovals between Q-1 and Q-2, and Q-3 and Q-4, respectively. In this hypothetical square grid with one diagonal topology, crosstalk occurs in all three edges marked with a flash, as they directly connect the qubits of these two operations.

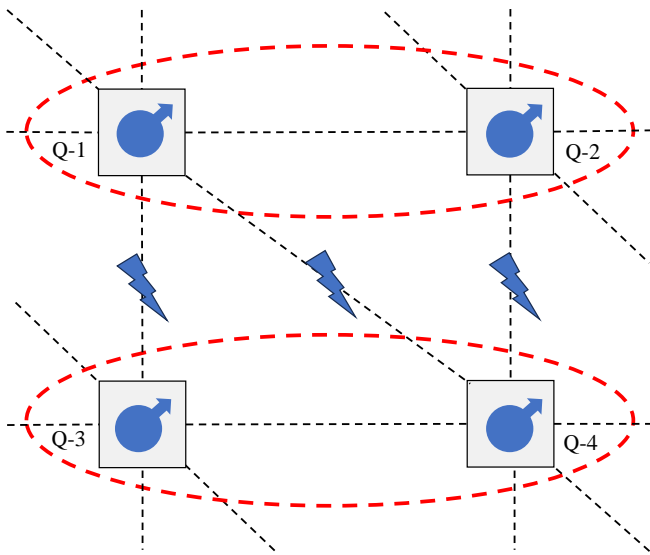


FIG. 3: Schematic overview of cross-talk when executing two-qubit gates. Dashed black lines indicate a direct connection between two qubits, the red ovals indicate an ongoing two-qubit gate, and the blue flash icons indicate contributing crosstalk effects.

### C. Decoherence term

The last term of Equation 2 represents the decoherence of quantum information; hence, it creates a strong trade-off between parallelization and crosstalk effects. Since  $N$  and  $T_2$  are given, we need to define the duration time of the circuit  $t$ :

$$t = \sum_{k=1}^M \max(D_{i,k}) \quad (5)$$

where  $D_{i,k}$  is the duration of the  $i$ th operation in the  $k$ th time step. In Table II, we present the gate duration and decoherence time used. The motivation behind this selection of durations, once again, is for purposes of architectural comparisons. We took reference for our two-qubit gate (i.e.,  $\sqrt{SWAP}$ ) from [43, 69], for the *Shuttle* from [27] which is half the shuttle-based Z rotations [46], for the pulsed-based single-qubit gates from [48], and the  $T_2$  from [28].

TABLE II: Overview of all gate duration and the decoherence time used.

Operation	Shuttle	X/Y/Z (Pulse)	Z (Shuttle)	$\sqrt{SWAP}$	$T_2$
Duration (ns)	10	100	20	200	1,000,000

## VI. ARTA (ARTIFICIAL ARCHITECT)

From the aforementioned transformation of the SpinQ compilation framework to a Design Space Exploration (DSE) framework, we are able to brute force through all valid combinations of the input variable values. However, as we discussed, this can be a time-consuming process, especially when the defined design space is large. Therefore, a specialized tool is needed to automate the DSE process by traversing the space in a clever and faster way. Ultimately, this will result in fewer designs being tried until desired ESP values or other metrics are reached.

To do that, we introduce ArtA, a tool built into the SpinQ framework containing multiple optimizers. Its goal is to give answers to (a) which optimization technique performs best on the task of finding an architecture that achieves the desired ESP and (b) which architecture provides the highest ESP, both per quantum circuit.

The abstracted ArtA process is depicted in Figure 4. The initialization of ArtA starts with one or more quantum circuits, a design space such as the one described in Sec. IV, the optimization method(s) to traverse the space, and an (optional) termination condition. Inside the optimization stage, ArtA provides an architecture and circuit to SpinQ for compilation, gets the ESP value, and, based on a policy of the optimization method, selects the next architecture (in the form of input variable values) from the available “population” of architectures – a subset of the complete design space determined by the optimization algorithm itself. This process repeats until a specific termination condition (TC) (e.g., elapsed time) is met or a desired value of a specific metric is reached (in this work, ESP). Upon termination, the resulting architecture, its ESP, and ArtA metrics are stored. In the following sections, we will describe the TC and ArtA metrics.

In the Appendix XB, we analytically discuss the five optimization methods used and their hyper-parameter variations, totaling seventeen different optimization configurations. Also, in the Appendix XA, we present the seven benchmark quantum circuits and their different sizes in terms of qubit counts.

To answer the last two research questions, we will use ArtA’s (a) and (b) capabilities. In the first one, we answer the third research question by testing all the implemented optimization methods to determine which finds the highest ESP the fastest for each quantum circuit. Therefore, we will compile each circuit for all 29,312 architectures and store their ESP. Then, we can run each method and determine the methods’ performance based on two new metrics introduced in Sec. VIB evaluating ArtA’s overall performance. In the second way, we will only use the best-performing optimization

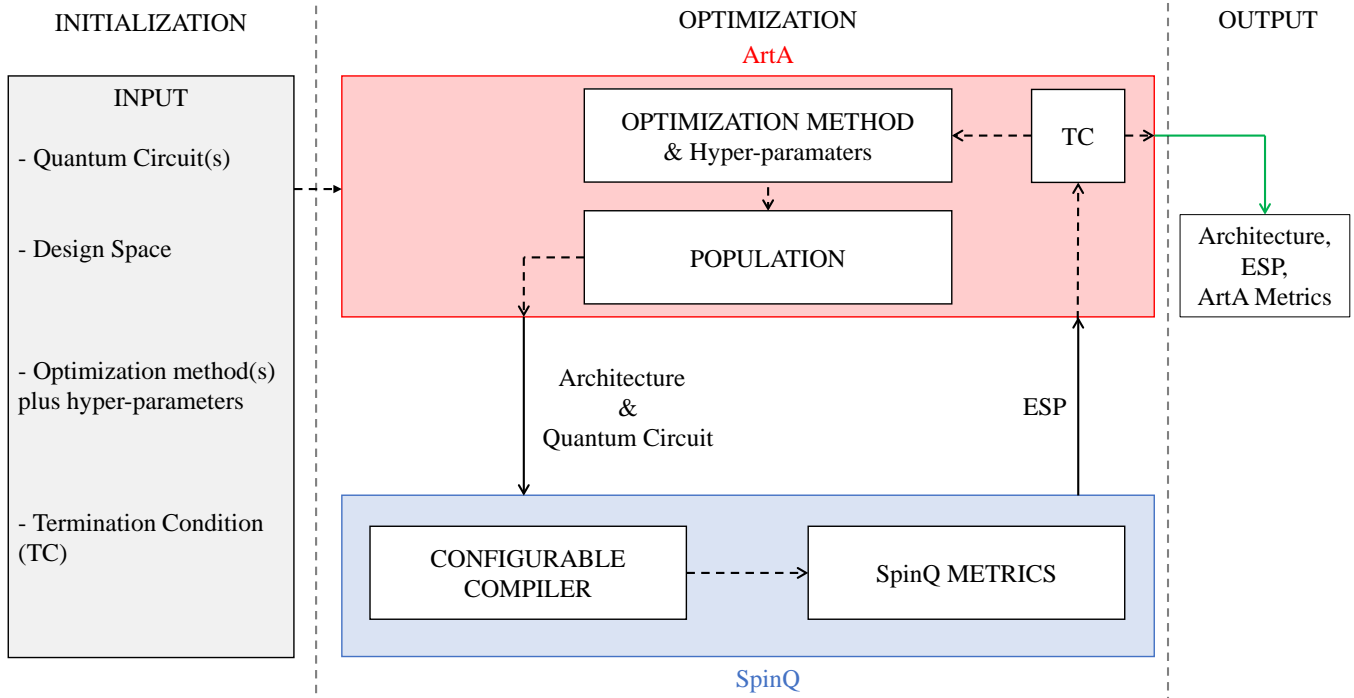


FIG. 4: Schematic overview of the initialization, optimization, and output cycle of ArtA (red box) with SpinQ (blue box).

method but expand our circuit selection to concretely answer the last research question.

#### A. Termination Condition (TC)

During each optimization cycle, a specific termination condition (TC) is checked to reduce further computational time based on the way ArtA is used. Since we already obtained the ESP values for all architectures first during the third question, the highest ESP is known and can work as a TC. Additionally, we observed in practice that most runs reach the highest ESP sooner than 40 minutes; hence, this can be another TC. More specifically, our analysis revealed that over 95% of processes are completed earlier, while a minority extends significantly longer. Given that our evaluation focuses on runtime, omitting these prolonged instances won't affect the overall assessment, as their inclusion would lead to unfavorable evaluations regardless.

Therefore, the TC when answering the third research question is:

- If the highest ESP value is found.
- If the method's run time exceeds 40 minutes.

For the second use of ArtA, which answers the fourth research question, we investigate the returned architectural designs by using the chosen optimization method derived from answering the third question. We find in practice that the corresponding chosen optimization algorithm did not exceed trying 23.4% of the total 29,312 architectures in the worst case before finding the one with the highest ESP.

Therefore, when answering the last research question, the TC triggers:

- When the number of evaluated architectures exceeds 23.4% of the total 29,312.

#### B. Metrics Evaluating ArtA

To determine the performance of ArtA in the context of replying to the third research question, we need to define some relevant metrics. The optimization methods that will eventually determine ArtA's performance should return a desired solution faster compared to searching with the brute-force approach. Otherwise, ArtA will be of no practical interest. We thus use the relative *time-to-solution* as a metric in Equation 6. The numerator includes the total runtime of both the optimization method and compilation until the desired result is reached (or the TC is triggered), and the denominator refers to the total runtime to brute force the entire design space.

$$\text{time-to-solution}_{\text{relative}} = \frac{\text{time-to-solution}}{T_{\text{Brute-force}}} \cdot 100\% \quad (6)$$

When the average compilation time increases due to larger quantum circuits, the execution time of the optimization method slowly becomes less important within the total runtime. Because of that, *time-to-solution* is not sufficient in evaluating ArtA's performance. Thus, a relative *calls-to-solution* metric, in Eq. 7, is also a strong performance predictor for ArtA, especially for larger circuits. With *calls-to-solution* in

the numerator, we refer to the total number of times SpinQ is called to compile for each new architecture. In case the optimization method attempts the same architecture twice or more, the compilation will be skipped since the results are already stored from the first call. Finally, the denominator represents the brute force approach and is the total number of architectures in the design space, which essentially equals 29,312.

$$\text{calls-to-solution}_{\text{relative}} = \frac{\text{calls-to-solution}}{N_{\text{architectures}} = 29,312} \cdot 100\% \quad (7)$$

## VII. RESULTS AND EVALUATION

In this section, we will attempt to completely answer the third and fourth search questions. In both questions, we will focus on finding the architecture that obtains the highest ESP among all in the design space. However, before that, we briefly detail our experimental setup. Since all optimization methods are inherently probabilistic, multiple runs are required to create robust conclusions. Due to limited computational resources<sup>2</sup>, we ran each method for each hyper-parameter combination ten times alongside the TC. Besides the *mean* performance, we will also report the *worst* performing results for reference.

### A. Comparison of optimization methods

In this first part of our results, we will address the third research question stated in Section III, which is about finding the best performing optimization method according to our ArtA metrics defined in Section VIB. The results of the relative *time-to-solution* metric for finding the architecture with the highest ESP are given in Table III. This table also provides insights into matching different method configurations (described in Appendix XB) with specific quantum circuits. As explained previously, the denominator of Eq. 6 is obtained beforehand by measuring the time taken by the brute force approach. We observe overall that for each quantum circuit, on average, all optimization methods find the solution in less time than brute-forcing (values under 100). For a better interpretation of the numbers on the table, a 50 means the particular optimization configuration of ArtA takes half the time of brute forcing all architecture, and 100 means that it takes the same time.

Multiple optimization methods greatly outperform the random sampling (RS column), as expected. The best performance is at **0.9%** on average for QV10 with SA [20, 3], meaning that ArtA, with this optimization method configuration

and quantum circuit, takes only **0.9%** on average of the total brute force time to find the architecture with the highest ESP.

We calculated based on Table III that, on average, for all optimization methods, ArtA was able to decrease the exploration time by **80.6%**. Overall, different optimization methods clearly show varied performance across their respective columns. However, the performance differences among various hyper-parameter settings within a single optimization method are less distinct. In a performance order, we can observe GA being first, followed by BO, ACO, and, lastly, SA. More specifically, GA, with a population size of 50 and a mutation probability of 0.15, finds the highest ESP the fastest at **11.9%** relative *time-to-solution*, on average, with BO [EI, MA] coming close at **12.1%**. Lastly, in **86.7%** of the cases, a top 5 optimization method configuration in the *worst* row is also a top 5 optimization method configuration in the **mean** row, which indicates the consistency of the results. To further support our findings, next, we will assess the relative *calls-to-solution* metric.

The results of the relative *calls-to-solution* metric for reaching the highest ESP are given in Table IV. We observe overall that for each quantum circuit, all optimization methods were able to find the highest ESP architecture in fewer compiler calls than brute-forcing through all 29,312 architectures. Once again, for a better interpretation of the numbers on the table, 50 means the particular optimization configuration of ArtA needs to go through half the architectures in the design space, and 100 means it needs to go through all the architectures.

The best optimization method only takes **1%** of the total compiler calls, on average, for QV8 and QV10 with ACO [50, 0.1]. We calculated based on Table IV that, on average, ArtA's optimization method configurations can decrease the compiler calls by **79.9%**. We can observe, once again, that BO, followed by GA, obtained the best performance compared to other optimization methods. Lastly, in **91.7%** of the cases, a top 5 optimization method configuration in the *worst* row is also a top 5 optimization method configuration in the **mean** row, showing results consistency again.

From the different variants of the GA and BO used, we focus on GA [100, 0.2] and BO [EI, MA], as they have the best performance and did not reach our TC in any of the ten runs. By comparing the two tables, we can observe that BO [EI, MA] needs marginally more time to evaluate fewer architectures compared to GA [100, 0.2]. Since the compilation time per architecture is the same between methods, this points to a slightly (0.2% on average) longer execution time of BO [EI, MA] compared to GA [100, 0.2]. This can be explained based on the algorithm's reliance on matrix multiplication and several other linear algebra operations, which are computationally more expensive than the more simple operations of GA (see Sec. XB). However, the actual total runtime of ArtA will depend on the ratio between compilation and optimization time, which can change for large circuits. Based on their small relative *time-to-solution* difference, we can predict that BO [EI, MA] will outperform GA [100, 0.2] for larger circuits as the latter has, on average, 58% higher relative *calls-to-*

<sup>2</sup> All time metrics were retrieved by running ArtA with Python 3.10.8 single-threaded on a 2017 MacBook Pro, using a 3.1 GHz Quad Core Intel i7 processor and 16 GB of RAM.

Circuits\Methods		RS	SA				BO				GA				ACO				
			20 2	20 3	50 3	50 2	UCB Ma	EI Ma	EI Ga	UCB Ga	50 0.15	50 0.2	100 0.2	100 0.15	50 0.1	100 0.3	100 0.1	50 0.3	
QFT	10	mean	53.9	45.4	61.8	45.2	54.9	22.5	15.0	22.6	17.0	30.3	33.8	21.4	44.5	24.4	40.5	28.1	28.6
		worst	98.2	87.6	99.8	98.9	100.4	55.0	35.4	38.5	-	-	88.7	46.1	132.8	58.7	96.9	58.6	60.6
	20	mean	47.3	17.8	44.6	47.4	33.6	10.9	10.8	11.5	6.9	6.3	6.8	9.2	5.4	36.5	48.7	31.9	42.6
		worst	96.8	50.5	84.2	93.1	57.0	25.6	25.8	28.2	21.4	15.7	12.8	15.6	16.6	59.2	87.9	60.8	80.7
cA	5b	mean	35.7	38.0	41.8	36.5	27.0	16.2	10.0	14.3	7.1	8.4	6.8	4.8	5.2	15.5	11.5	18.2	14.9
		worst	58.1	67.1	93.0	71.8	64.6	61.0	27.4	33.9	22.1	16.9	14.5	9.2	12.6	33.5	26.6	73.1	43.0
	10b	mean	37.3	8.4	22.6	25.8	28.7	4.2	11.3	8.1	12.5	4.3	3.5	5.0	3.9	24.1	11.7	24.7	18.3
		worst	86.0	37.5	72.2	89.8	76.8	12.4	28.3	21.7	30.0	8.0	7.6	12.8	9.5	61.4	27.8	63.5	41.4
vA	5b	mean	52.3	10.0	24.9	18.3	11.8	10.4	9.2	9.0	7.4	3.1	5.8	5.9	4.5	15.6	12.6	18.0	22.8
		worst	80.2	23.6	56.5	31.2	29.9	21.7	22.3	19.9	29.1	8.5	12.2	13.8	10.6	38.5	42.8	61.9	44.7
	10b	mean	46.7	33.4	46.9	52.1	38.0	5.4	5.0	8.0	3.7	9.2	9.4	8.9	7.2	28.1	26.2	32.4	47.4
		worst	98.3	70.4	79.5	81.6	79.8	12.8	15.9	21.5	7.1	15.4	15.8	18.5	17.1	59.6	52.2	79.6	75.9
QV	8	mean	40.0	7.9	2.4	5.5	4.9	16.0	17.0	56.3	74.4	29.0	40.5	29.6	37.9	1.1	1.3	1.3	1.8
		worst	71.4	26.0	7.9	20.9	19.6	-	38.6	-	-	-	74.9	72.6	-	2.1	3.0	1.9	6.7
	10	mean	63.7	3.4	0.9	2.8	2.6	21.6	13.3	32.2	67.4	20.4	19.4	12.5	19.4	1.0	1.3	1.1	1.3
		worst	91.3	10.4	2.7	11.0	9.4	-	33.9	55.4	-	42.8	37.9	39.5	39.6	1.8	2.4	2.2	3.4
G	10	mean	43.2	56.8	46.0	51.8	46.6	42.1	30.6	30.6	45.5	27.0	14.2	26.8	32.1	23.3	18.1	34.2	27.8
		worst	80.4	98.3	97.4	101.1	91.6	81.7	70.4	59.4	103.6	58.3	33.0	42.6	74.2	79.2	41.8	65.1	52.5
	20	mean	62.1	46.1	59.6	34.3	46.5	11.5	12.1	11.8	7.1	7.5	8.9	11.7	13.0	30.4	24.2	26.9	32.4
		worst	96.1	85.6	92.2	84.6	85.7	34.4	33.4	25.3	17.4	17.4	23.2	21.9	25.9	57.6	52.6	81.5	80.6
R	8	mean	48.5	2.4	2.9	3.2	2.3	8.7	6.0	5.9	4.7	1.1	1.4	1.8	1.6	2.4	4.5	3.0	2.8
		worst	84.8	8.6	6.2	10.3	6.8	28.4	18.8	14.3	15.6	2.0	2.1	2.3	2.2	4.9	7.5	7.0	7.2
	10	mean	56.4	29.2	19.2	38.9	14.7	7.4	4.6	7.1	5.2	5.8	6.8	5.5	7.8	22.6	24.0	19.9	24.2
		worst	99.2	91.5	62.7	87.6	60.7	29.7	18.9	14.6	16.0	20.6	20.2	18.7	29.5	49.9	69.9	67.7	44.4
average	mean	48.9	24.9	31.1	30.2	26.0	14.7	12.1	18.1	21.6	12.7	13.1	11.9	15.2	18.8	18.7	20.0	22.1	
	worst	86.7	54.8	62.9	65.2	56.9	36.3	30.8	30.2	29.1	20.6	28.6	26.1	33.7	42.2	42.6	51.9	45.1	

TABLE III: Relative *time-to-solution* metric (the lower, the better) for finding the architecture with the highest ESP from the design space. A minus symbolizes that there was at least one run (out of the ten) in which the top ESP value was not reached in time (TC = 40 minutes). These results are colored red, as well as runs where the time taken exceeds the brute force time (values over 100). The green cells indicate the top five configurations of optimization methods for a given quantum circuit. The **mean** and **worst** performing configurations from a sample of ten runs are shown for each quantum circuit (block of rows). **QFT**: Quantum Fourier Transformation, **cA**: Cuccaro Adder, **vA**: vbe Adder, **QV**: Quantum Volume, **G**: Grover's, **RC**: Random Circuit, **RS**: Random Sampling, **SA**: Simulated Annealing (Top: Start Temperature, bottom: Step Size), **BO**: Bayesian Optimization (Top: Acquisition function, bottom: Kernel), **GA**: Genetic Algorithm (Top: Population Size, bottom: Mutation), **ACO**: Ant Colony Optimization (Top: Population Size, bottom: Exploitation Rate).

Circuits\Methods		RS	SA				BO				GA				ACO				
			20 2	20 3	50 3	50 2	UCB Ma	EI Ma	EI Ga	UCB Ga	50 0.15	50 0.2	100 0.2	100 0.15	50 0.1	100 0.3	100 0.1	50 0.3	
QFT	10	mean	53.9	46.1	61.8	45.2	55.3	9.0	6.4	9.0	7.6	23.1	28.9	23.1	22.0	24.9	38.3	29.3	26.8
		worst	98	87.2	98.5	97.5	98.9	18.6	12.8	13.8	-	-	63.1	43.5	51.2	56.8	79.5	58.6	54.4
	20	mean	47.3	18.7	44.7	47.7	35.2	9.7	9.6	10.6	6.4	8.1	8.8	11.8	6.9	38.4	49.3	34.0	42.6
		worst	96.8	51.6	84.2	92.9	59.1	21.3	22.5	24.2	18.8	19.6	16.3	19.4	20.2	61.8	84.7	63.9	77.1
cA	5b	mean	35.7	39.0	42.2	36.7	28.1	8.3	5.6	7.0	3.9	9.7	8.6	6.5	6.7	16.2	12.1	18.8	15.0
		worst	58.1	67.9	92.5	71.6	65.7	33	15	13.7	9.9	17.8	17.7	12.1	15.3	35.1	28	72.4	41
	10b	mean	37.4	9.0	22.8	26.0	29.6	3.8	8.6	6.5	9.7	5.8	4.7	6.7	5.2	24.5	12.0	25.5	18.7
		worst	85.9	39.2	72.4	89.8	77.3	10.4	21.9	15.9	24.2	10.6	10.1	16.5	12.3	62.8	29.4	66.1	42.1
vA	5b	mean	52.3	10.7	24.9	18.2	12.6	7.1	5.8	5.9	5.0	4.1	7.6	7.8	5.9	16.7	13.6	19.2	23.4
		worst	80.2	24.9	56.5	31.1	31.1	16.0	12.3	11.5	15.8	10.8	15.4	18.0	13.2	42.0	46.0	64.3	44.3
	10b	mean	46.7	34.6	46.5	51.7	39.0	5.5	4.9	7.9	4.3	12.0	12.5	11.5	9.3	29.2	27.1	33.5	47.5
		worst	98.3	71.5	79.1	81.1	80.5	12.1	14.7	19.5	7.5	18.9	20.1	23.0	20.9	61.5	53.9	80.8	73.4
QV	8	mean	40.0	8.1	2.4	5.6	5.0	11.0	12.0	35.2	48.3	21.1	37.3	28.6	28.1	1.0	1.3	1.3	2.0
		worst	71.3	26.4	8.2	21.4	19.8	-	30.0	-	-	-	66.1	65.9	-	2.0	3.3	2.1	7.7
	10	mean	63.7	3.5	0.9	2.9	2.7	18.6	11.1	25.9	55.4	20.8	20.6	13.4	19.9	1.0	1.2	1.0	1.2
		worst	91.1	10.8	2.8	11.3	9.7	-	28.5	43.3	-	40.5	39.5	41.3	38.9	2.0	2.3	2.1	2.9
G	10	mean	43.1	57.3	46.1	51.7	47.6	16.3	11.6	11.6	17.1	22.4	16.5	29.5	26.1	24.0	19.2	36.3	27.0
		worst	80.4	97.0	96.4	99.4	91.3	31.8	23.4	20.2	34.2	39.6	37.1	44.1	47.9	73.2	43.3	65.6	48.6
	20	mean	62.0	46.8	59.6	34.5	47.4	9.2	9.0	9.3	6.2	9.7	11.3	15.1	15.5	32.9	25.6	28.6	32.5
		worst	96.2	85.7	91.7	84.5	85.6	25.9	22.4	17.9	13.2	20.7	28.1	27.5	28.5	60.6	54.3	82.2	74.9
R	8	mean	48.4	2.8	3.2	3.4	2.7	7.4	5.5	5.3	4.4	1.5	1.9	2.4	2.1	3.4	6.2	4.2	3.7
		worst	84.7	9.4	6.3	11.0	7.6	21.7	17.2	11.3	13.6	2.9	2.9	3.1	3.1	6.9	10.4	10.1	9.8
	10	mean	56.4	29.9	19.7	39.1	15.5	7.2	4.4	6.8	5.3	6.7	8.5	6.8	8.9	24.9	25.6	21.5	25.9
		worst	99.2	91.6	63.2	87.6	61.9	26.6	17.1	12.9	14.9	23.1	23.9	22.5	31.0	53.5	70.6	71.0	46.2
	average mean	48.9	25.5	31.2	30.2	26.7	9.4	7.9	11.8	14.5	12.1	13.9	13.6	13.1	19.8	19.3	21.1	22.2	
	average worst	86.7	55.3	62.7	64.9	57.4	21.7	19.8	18.6	16.9	20.5	28.4	28.1	25.7	43.2	42.1	53.3	43.5	

TABLE IV: Relative *calls-to-solution* metric (the lower, the better) for finding the architecture with the highest ESP from the design space. A minus with red color cells symbolizes that there was at least one run (out of the ten) in which the top ESP value was not reached in time (TC = 40 minutes). The green cells indicate the top five configurations of optimization methods for a given quantum circuit. The **mean** and **worst** performing methods from a sample of ten runs are shown for each quantum circuit (block of rows). **QFT**: Quantum Fourier Transformation, **cA**: Cuccaro Adder, **vA**: vbe Adder, **QV**: Quantum Volume, **G**: Grover's, **RC**: Random circuit, **RS**: Random Sampling, **SA**: Simulated Annealing (Top: Start Temperature, bottom: Step Size), **BO**: Bayesian Optimization (Top: Acquisition function, bottom: Kernel), **GA**: Genetic Algorithm (Top: Population Size, bottom: Mutation), **ACO**: Ant Colony Optimization (Top: Population Size, bottom: Exploitation Rate).

*solution*. Therefore, we conclude that BO [EI, MA] is a better candidate for automating the DSE process for large-scale circuits, as it can traverse the design space faster.

Having said that, making a more detailed analysis for each circuit where internal circuit characteristics are correlated [2, 46] to optimization methods can improve the performance of ArtA by picking methods more accurately. This promising avenue is left for future work when more progress in circuit characterization is made.

## B. Architecture Analysis

We move on to address the last research question after having selected the best-performing optimization method in the previous section. Here, we use ArtA to create architectural insights into spin-qubit devices for each circuit category and suggest a universal architecture for all executed circuits.

In Table V, we present the values of the architectural variables, introduced in Sec. IV, that were found by ArtA having the highest ESP with the BO [EI, MA] optimization method alongside their ESP values. These circuits are organized by class and size in number of qubits within the rows of the table. Subsequent columns present the ESP of the best architecture discovered, followed by color-coded architectural parameter categories as delineated in Sec. IV. The use of color accents in the table serves to enhance visual clarity, with each corresponding to the values of each variable.

Before focusing on the architectural insights, we should comment on the low ESP values observed, especially in larger circuit sizes. Although such low values do not have any physical meaning after a certain small number, ESP still remains a reliable way to rank architectures. It’s important to understand ESP is not inherently random, regardless of how low it gets. For instance, slight variations between two architectures causing a single gate difference will consistently and reliably be reflected through their ESPs. As long as numeric underflows are not caused, ESP remains a robust Figure of Merit for our purposes.

Observing the data presented in Table V, it becomes evident that there is a discernible structure to the values of architectural variables. Notably, many or all circuits exhibit strong preferences for certain variables. Following an implications discussion on the circuit performance of these strong architectural preferences, we will explore areas of weaker preference where there is more variability in value choices.

### Strong preference

First, we observe a unanimous preference for the Z rotation implementation (`z_rot_impl`) in the `zri` column, with a pulse-based rotation being preferred. Note that previously, we have assumed in Section VA that a shuttle and a pulse-based Z rotation share the same single-qubit gate fidelity, but because the latter requires two shuttles, it can benefit the ESP more than the other type. Moreover, as a shuttle operation involves two quantum dots while a pulse-based operation only involves one, the shuttle-based Z rotation will have a higher chance of incurring crosstalk errors based on our crosstalk definition. Given these two reasons, BO has favored the

shuttle-based version. This indicates that shuttle-based single-qubit rotations are not as sustainable as pulsed-based for large-scale circuits.

Moving on, the X, Y, and Z gates are implemented the same way hardware-wise, `xy_z` automatically is assumed 1 based on the interdependencies detailed in Section IV F. Consequently, `xy_tqg` and `z_tqg` are equivalent, taking both either 0 or 1 from the optimization method of ArtA (BO [EI, MA]), as we can observe in the table. Additionally, `xy_z_tqg` can also be conceptually equivalent to `xy_tqg` and `z_tqg` since the pulse-based Z rotation is selected. Therefore, whenever `xy_z_tqg` is 1 or `xy_tqg` and `z_tqg` is 1, it means the architecture(s) which allow(s) parallelization of all single- and two-qubit gates obtains the highest ESP. In that sense, one would expect `xy_z_tqg`, `xy_tqg` and `z_tqg` to be synchronized. However, since such exploration freedom was given in the design space, the reasons for the mismatches could be explained by the internal characteristics of the circuits themselves. For example, in QFT100, the parallelization of all gate types occurs more often than in QFT60, which has `xy_z_tqg` = 0, `xy_tqg` = 1, and `z_tqg` = 1.

Conversely, when applying the same reasoning to QV8, QV10, and QFT20, it is not necessary for the hardware to support parallel executions of single-qubit and two-qubit gates. This shows that the success of real quantum circuits can come from different “angles” with reduced hardware capabilities<sup>3</sup>.

Another strong preference appears in the beSnake router, observed by the dark green 1 values in the `router` column. This result shows that the crosstalk implications of using the beSnake router (which gives more shuttling freedom) over the shuttle-based SWAP router (which minimizes crosstalk) are not as important as the other two components in Equation 2. Similarly, the `degree` variable is mostly maximized, indicating again that the additional possibility of crosstalk does not outweigh other benefits, such as having more connections to perform two-qubit gates and shuttling operations.

Lastly, there is a strong preference for a local single-qubit gate implementation (`single_qubit_impl`). A local implementation, on the one hand, provides the highest parallelization possibilities, but on the other, it is the most demanding to achieve experimentally on real hardware.

Based on all the above conclusions, we can summarize that the crosstalk effect is not as strong even though ArtA suggests architectures with high crosstalk factors (the highest connectivity and parallelization and the most dense routing strategy). In fact, the decoherence-induced errors increase more severely (exponentially) with time, based on Equation 4, than crosstalk, especially in circuits with high qubit and gate counts, which explains the prevailing preference for maximizing parallelization.

The same can be observed in our universal architecture recommendation in the last row, which performs best on average

<sup>3</sup> Ultimately, each circuit profile has specific architectural traits that can be leveraged to achieve optimal performance without the need for excessively advanced hardware features (achieving a balance in architectural characteristics).

Circuit	Gate count	ESP	xy_z	xy_tqg	z_tqg	xy_z_tqg	xyD	zD	tqgD	sD	sqi	zri	router	swap opt	degree
QFT10	205	58.02	1	1	1	1	100	50	75	100	1	1	1	1	8
QFT20	810	1.12	1	0	0	0	25	100	25	75	1	1	1	0	8
QFT40	4072	3.54E-15	1	0	0	1	100	25	1	25	1	1	1	0	8
QFT50	5025	1.50E-32	1	1	1	0	75	25	100	75	1	1	1	0	8
QFT60	7230	6.37E-59	1	1	1	0	100	50	25	50	1	1	1	0	8
QFT100	20050	6.80E-123	1	0	0	1	100	75	50	100	1	1	1	1	8
G10	278	64.37	1	0	0	1	25	50	1	25	1	1	1	1	8
G20	668	12.31	1	0	0	1	75	25	25	100	1	1	1	1	8
G50	1838	1.11E-05	1	1	1	1	75	50	100	25	1	1	1	1	8
G80	3008	9.55E-18	1	1	1	1	50	50	1	100	1	1	1	0	8
G90	3398	2.28E-23	1	1	1	1	100	100	1	25	1	1	1	0	8
G100	3788	3.88E-30	1	1	1	0	100	75	50	100	1	1	1	0	8
G150	5738	2.71E-75	1	1	1	1	25	25	75	50	1	1	1	0	8
G200	7688	1.56E-144	1	1	1	0	75	50	75	25	1	1	1	0	8
cA12	31	61.51	1	0	0	1	75	75	75	100	1	1	1	0	8
cA22	61	19.29	1	0	0	1	75	25	25	75	1	1	1	1	8
cA42	121	0.13	1	0	0	1	100	50	50	75	1	1	1	0	8
cA62	181	2.24E-05	1	0	0	1	75	100	100	100	1	1	1	0	8
cA82	241	1.54E-10	1	0	0	1	100	50	100	100	1	1	1	0	8
cA100	295	3.82E-16	1	0	0	1	50	100	75	100	1	1	1	0	8
cA130	385	4.67E-30	1	0	0	1	50	75	1	100	1	1	1	0	8
cA258	769	1.56E-137	1	0	0	1	100	75	100	75	1	1	1	0	8
vA16	36	41.06	1	0	0	1	75	75	1	50	1	1	1	1	8
vA31	76	3.03	1	1	1	0	100	100	25	25	1	1	1	1	8
vA61	156	2.90E-05	1	0	0	1	50	100	50	75	1	1	1	1	8
vA91	236	3.97E-13	1	0	0	1	50	100	100	25	1	1	1	0	8
vA121	316	1.46E-25	1	0	0	1	50	100	100	50	1	1	1	0	8
vA148	388	3.57E-40	1	0	0	1	100	100	75	25	1	1	1	0	8
vA193	508	5.42E-71	1	0	0	1	50	100	25	25	1	1	1	0	8
QV8	889	50.50	1	0	0	0	-1	-1	1	25	2	1	1	1	8
QV10	1111	38.55	1	0	0	0	-1	-1	1	25	2	1	1	1	8
QV20	4408	4.35	1	0	0	1	50	100	50	100	1	1	1	1	8
QV30	9939	1.42E-03	1	0	0	1	100	100	50	100	1	1	1	0	8
QV40	9939	3.87E-11	1	0	0	1	100	100	50	50	1	1	1	1	8
bV11	24	97.61	1	0	0	0	-1	-1	100	100	2	1	1	1	8
bV21	44	95.22	1	0	0	0	-1	-1	1	100	2	1	1	1	6
bV30	62	92.73	1	0	0	0	-1	-1	100	100	2	1	1	0	8
bV40	82	89.84	1	0	0	0	-1	-1	100	75	2	1	1	1	8
bV50	102	86.68	1	0	0	0	-1	-1	100	100	2	1	1	1	8
bV65	132	81.86	1	0	0	0	-1	-1	100	50	2	1	1	1	6
bV129	261	46.57	1	0	0	0	-1	-1	25	75	2	1	1	0	8
bV257	519	3.78	1	0	0	0	-1	-1	25	25	2	1	1	1	8
Average (universal architecture)			1.0	0.2	0.2	0.6	74.2	71.1	52.6	66.7	1.2	1.0	1.0	0.5	7.9

TABLE V: Architectures returned by ArtA with BO [EI, MA] optimization method for a range of quantum circuits. Results are color-coded, with color schemes following the categories introduced in Section IV.

for all the circuits examined. Additionally, the operational fidelity, which is directly linked to the gate overhead of compilation, can also severely impact the final ESP for circuits with high gate counts, which in turn explains the need to add the least additional gates possible during compilation through the use of beSnake [45] and local single-qubit implementa-

tion. Having said that, Bernstein Vazirani, QV8, and QV10 circuits preferred the global implementation, as these circuits consist of a significant number of similar single-qubit gates being executed at the same time step.

#### Weak preference

Overall, we can observe that the single-qubit operations

and shuttling prefer a higher degree of parallelization than the two-qubit gates. Considering that  $x_{yD}$  and  $zD$  have the same meaning, their combined averages (excluding -1 values) from the last row of Table V is **72.7%** and the  $sD$  to **66.7%**. This compares to an average of **52.6%** for the two-qubit gates. Therefore, prioritizing the simultaneous operation of single-qubit gates (and shuttling) over two-qubit gates is more important in spin-qubit architectures.

The `swap_opt` variable seems to show a preference for supporting SWAP gates for lower qubit counts. A possible explanation for this is that SWAP operations take a longer time than a parallelized sequence of shuttles [45]. As we explained before, the effects of having longer circuit execution times become more severe with larger circuits; hence, the extra SWAPs can outweigh the gained fidelity they initially offer. Combining this conclusion for large-scale circuits and the strong preferences for shuttling freedom (beSnake router) indicates that the shuttle operation is a key communication method for spin-qubit devices.

## VIII. ACKNOWLEDGEMENT

This work is part of the research program OTP with project number 16278, which is (partly) financed by the Netherlands Organisation for Scientific Research (NWO). CGA acknowledges funding from the Spanish Ministry of Science, Innovation and Universities through the Beatriz Galindo program 2020 (BG20-00023) and from the European ERDF under grant PID2021-123627OB-C51.

## IX. CONCLUSION

In this paper, we propose a comprehensive exploration of the current and future architectural design space for spin-qubit-based quantum dots quantum processors. Our research focuses on assessing the critical architectural characteristics that could be key in ensuring high performance on such devices. To this end, we present an upgraded version of the SpinQ compilation framework for spin qubit architectures in which architectural variables can configure internal compilation passes, making it the first Design Space Exploration (DSE) framework. After defining our design space, consisting of 29,312 architectures, we propose a multi-optimization-based tool, ArtA (Artificial Architect), to automate the DSE process. The goal of ArtA is (a) to suggest which of the seventeen optimization method configurations can find the architecture with the highest ESP the fastest compared to the brute forcing approach and (b) which architectural design characteristics are key for building high-performance spin-qubit devices per circuit category. We have shown up to **99.1%** improvement in computation times compared to the brute-force approach. We have also provided insights into matching different optimization methods with specific quantum circuit categories. Bayesian optimization with an Expected Improvement acquisition function and a Matérn kernel was chosen as the best optimization method due to its effectiveness in man-

aging higher qubit counts. After that, we proceed to automate the DSE process for 44 quantum circuits of up to 258 qubits within the 29,312-architecture design space. Our findings reveal the importance of minimizing the circuit duration by maximizing parallelization whenever possible instead of selecting architectural characteristics that minimize crosstalk errors. Crosstalk is currently a significant concern in experiments, but our long-term considerations deem decoherence more crucial. Lastly, the shuttle operation is preferred over costly SWAP operations for communication purposes, especially for large-scale circuits. Contrary to that, shuttle-based single-qubit gates such as Z rotations are not preferred over pulsed-based. Furthermore, our universal architecture suggestion places higher priority on parallelizing single-qubit gates rather than two-qubit gates.

As for future improvements, a broader range of hyperparameter combinations and circuit variations could enhance ArtA’s effectiveness. Then, with advancements in spin qubit device fabrication, new architectural variables, and values could potentially update the design space, and such integration will be relatively straightforward owing to the modularity of the internal functions of SpinQ and ArtA. Moreover, introducing non-architectural constraints such as development costs and time into ArtA’s design space could help make real-world conclusions regarding developing spin qubits. This would allow for operational fidelities to become variables as well and, consequently, add a second dimension to the Figure of Merit (ESP).

Also, some of the assumptions made in this work could be fine-tuned as the field progresses. It is crucial to acknowledge the impact of these assumptions on the observations presented. For instance, we assumed that the fidelity of pulse-based Z rotations is equivalent to that of a single shuttle operation. This assumption should not be construed as either favorable or unfavorable; rather, it is a foundational premise upon which ArtA bases its architectural “recommendations”. Should empirical evidence later demonstrate that shuttle operations exhibit significantly higher fidelity compared to pulse-based Z rotations or the crosstalk model depends on more factors, it may necessitate a reevaluation of preferences.

Further analysis of architectural patterns with similar quantum circuit characteristics can reveal more trends. For instance, quantum circuits with high two-qubit gate percentage ranges can perform best when the qubit connectivity of the architecture is above a certain degree. These kinds of statements or more can be made for a plethora of circuit characteristics [2, 46] and, in doing so, create a general matching between algorithm categories and architectural designs. Once this is done, it is possible to make the reversed suggestion of which architecture will perform best for an input circuit of interest once categorized without needing to repeat the DSE process.

- [1] Carmen G Almudever and Eduard Alarcon. 2021. Structured optimized architecting of full-stack quantum systems in the nisq era. In *2021 Design, Automation & Test in Europe Conference & Exhibition (DATE)*. IEEE, 762–767.
- [2] Medina Bandic, Carmen G Almudever, and Sebastian Feld. 2023. Interaction graph-based characterization of quantum benchmarks for improving quantum circuit mapping techniques. *Quantum Machine Intelligence* 5, 2 (2023), 40.
- [3] Ethan Bernstein and Umesh Vazirani. 1993. Quantum complexity theory. In *Proceedings of the Twenty-Fifth Annual ACM Symposium on Theory of Computing (STOC '93)*. Association for Computing Machinery, New York, NY, USA, 11–20. <https://doi.org/10.1145/167088.167097>
- [4] Hendrik Bluhm and Lars R Schreiber. 2019. Semiconductor spin qubits—A scalable platform for quantum computing?. In *2019 IEEE International Symposium on Circuits and Systems (ISCAS)*. IEEE, 1–5.
- [5] Francesco Borsoi, Nico W Hendrickx, Valentin John, Marcel Meyer, Sayr Motz, Floor Van Riggelen, Amir Sammak, Sander L De Snoo, Giordano Scappucci, and Menno Veldhorst. 2024. Shared control of a 16 semiconductor quantum dot crossbar array. *Nature Nanotechnology* 19, 1 (2024), 21–27.
- [6] Francesco Borsoi, Nico W Hendrickx, Valentin John, Sayr Motz, Floor van Riggelen, Amir Sammak, Sander L de Snoo, Giordano Scappucci, and Menno Veldhorst. 2022. Shared control of a 16 semiconductor quantum dot crossbar array. *arXiv preprint arXiv:2209.06609* (2022).
- [7] Jelmer M Boter, Juan P Dehollain, Jeroen PG Van Dijk, Yuanxing Xu, Toivo Hensgens, Richard Versluis, Henricus WL Naus, James S Clarke, Menno Veldhorst, Fabio Sebastiano, et al. 2022. *Physical Review Applied* 18, 2 (2022), 024053.
- [8] Guido Burkard, Thaddeus D Ladd, Andrew Pan, John M Nichol, and Jason R Petta. 2023. Semiconductor spin qubits. *Reviews of Modern Physics* 95, 2 (2023), 025003.
- [9] Leon C Camenzind, Simon Geyer, Andreas Fuhrer, Richard J Warburton, Dominik M Zumbühl, and Andreas V Kuhlmann. 2022. A hole spin qubit in a fin field-effect transistor above 4 kelvin. *Nature Electronics* 5, 3 (2022), 178–183.
- [10] Anasua Chatterjee, Paul Stevenson, Silvano De Franceschi, Andrea Morello, Nathalie P de Leon, and Ferdinand Kuemmeth. 2021. Semiconductor qubits in practice. *Nature Reviews Physics* 3, 3 (2021), 157–177.
- [11] Frederic T Chong, Diana Franklin, and Margaret Martonosi. 2017. Programming languages and compiler design for realistic quantum hardware. *Nature* 549, 7671 (2017), 180–187.
- [12] Rigetti Computing. 2019. Pyquil documentation. URL <http://pyquil.readthedocs.io/en/latest> (2019), 64–65.
- [13] D Coppersmith. 2002. *RC 19642 (07/12/94) Mathematics IBM Research Report An Approximate Fourier Transform Useful in Quantum Factoring*. Technical Report.
- [14] Andrew W Cross, Lev S Bishop, Sarah Sheldon, Paul D Nation, and Jay M Gambetta. 2019. Validating quantum computers using randomized model circuits. *Physical Review A* 100, 3 (2019), 032328.
- [15] Steven A Cuccaro, Thomas G Draper, Samuel A Kutin, and David Petrie Moulton. 2004. *A new quantum ripple-carry addition circuit*. Technical Report.
- [16] Nathalie P De Leon, Kohei M Itoh, Dohun Kim, Karan K Mehta, Tracy E Northup, Hanhee Paik, BS Palmer, Nitin Samarth, Sorawis Sangtawesin, and David W Steuerman. 2021. Materials challenges and opportunities for quantum computing hardware. *Science* 372, 6539 (2021), eabb2823.
- [17] Marco De Michielis, Elena Ferraro, Enrico Prati, Louis Hutin, Benoit Bertrand, Edoardo Charbon, David J Ibberson, and Miguel Fernando Gonzalez-Zalba. 2023. Silicon spin qubits from laboratory to industry. *Journal of Physics D: Applied Physics* 56, 36 (2023), 363001.
- [18] Cirq Developers. 2023. Cirq.
- [19] M Dorigo, M Birattari, and T Stutzle. 2006. Ant colony optimization. *IEEE Computational Intelligence Magazine* 1, 4 (2006), 28–39. <https://doi.org/10.1109/MCI.2006.329691>
- [20] David P Franke, James S Clarke, Lieven MK Vandersypen, and Menno Veldhorst. 2019. Rent’s rule and extensibility in quantum computing. *Microprocessors and Microsystems* 67 (2019), 1–7.
- [21] Peter I. Frazier. 2018. A Tutorial on Bayesian Optimization. (7 2018). <http://arxiv.org/abs/1807.02811>
- [22] Peter I Frazier. 2018. A tutorial on Bayesian optimization. *arXiv preprint arXiv:1807.02811* (2018).
- [23] Eduardo C Garrido-Merchán and Daniel Hernández-Lobato. 2020. Dealing with categorical and integer-valued variables in Bayesian Optimization with Gaussian processes. *Neurocomputing* 380 (2020), 20–35. <https://doi.org/10.1016/j.neucom.2019.11.004>
- [24] Lov K Grover. 1996. A Fast Quantum Mechanical Algorithm for Database Search. In *Proceedings of the Twenty-Eighth Annual ACM Symposium on Theory of Computing (STOC '96)*. Association for Computing Machinery, New York, NY, USA, 212–219. <https://doi.org/10.1145/237814.237866>
- [25] Ronald Hanson, Leo P Kouwenhoven, Jason R Petta, Seigo Tarucha, and Lieven MK Vandersypen. 2007. Spins in few-electron quantum dots. *Reviews of modern physics* 79, 4 (2007), 1217.
- [26] Irina Heinz and Guido Burkard. 2021. Crosstalk analysis for single-qubit and two-qubit gates in spin qubit arrays. *Physical Review B* 104, 4 (2021), 045420.
- [27] Jonas Helsen, Mark Steudtner, Menno Veldhorst, and Stephanie Wehner. 2018. Quantum error correction in crossbar architectures. *Quantum Science and Technology* 3, 3 (2018), 035005.
- [28] NW Hendrickx. 2021. Qubit arrays in germanium. (2021).
- [29] Nico W Hendrickx, William IL Lawrie, Maximilian Russ, Floor van Riggelen, Sander L de Snoo, Raymond N Schouten, Amir Sammak, Giordano Scappucci, and Menno Veldhorst. 2021. A four-qubit germanium quantum processor. *Nature* 591, 7851 (2021), 580–585.
- [30] Charles D Hill, Eldad Peretz, Samuel J Hile, Matthew G House, Martin Fuechsle, Sven Rogge, Michelle Y Simmons, and Lloyd CL Hollenberg. 2015. A surface code quantum computer in silicon. *Science advances* 1, 9 (2015), e1500707.
- [31] Intel Corporation. 2023. Intel’s New Chip to Advance Silicon Spin Qubit Research for Quantum Computing. <https://www.intel.com/content/www/us/en/newsroom/news/quantum-computing-chip-to-advance-research.html>.
- [32] Ali JavadiAbhari, Shruti Patil, Daniel Kudrow, Jeff Heckey, Alexey Lvov, Frederic T Chong, and Margaret Martonosi. 2014. ScaffCC: A framework for compilation and analysis of quantum computing programs. In *Proceedings of the 11th ACM Conference on Computing Frontiers*. 1–10.

- [33] Nader Khammassi, Imran Ashraf, JV Someren, Razvan Nane, AM Krol, M Adriaan Rol, Lingling Lao, Koen Bertels, and Carmen G Almudever. 2021. OpenQL: A portable quantum programming framework for quantum accelerators. *ACM Journal on Emerging Technologies in Computing Systems (JETC)* 18, 1 (2021), 1–24.
- [34] S Kirkpatrick, C D Gelatt, and M P Vecchi. 1983. *Optimization by Simulated Annealing*. Technical Report. 4598 pages.
- [35] Ruoyu Li, Luca Petit, David P Franke, Juan Pablo Dehollain, Jonas Helsen, Mark Steudtner, Nicole K Thomas, Zachary R Yoscovits, Kanwal J Singh, Stephanie Wehner, et al. 2018. A crossbar network for silicon quantum dot qubits. *Science advances* 4, 7 (2018), eaar3960.
- [36] Chia-Chun Lin, Amlan Chakrabarti, and Niraj K Jha. 2014. Qlib: Quantum module library. *ACM Journal on Emerging Technologies in Computing Systems (JETC)* 11, 1 (2014), 1–20.
- [37] Daniel Loss and David P. DiVincenzo. 1998. Quantum computation with quantum dots. *Phys. Rev. A* 57 (Jan 1998), 120–126. Issue 1. <https://doi.org/10.1103/PhysRevA.57.120>
- [38] Deepak M Mathew, André Lucas Chinazzo, Christian Weis, Matthias Jung, Bastien Giraud, Pascal Vivet, Alexandre Levisse, and Norbert Wehn. 2019. RRAMSpec: A design space exploration framework for high density resistive RAM. In *Embedded Computer Systems: Architectures, Modeling, and Simulation: 19th International Conference, SAMOS 2019, Samos, Greece, July 7–11, 2019, Proceedings 19*. Springer, 34–47.
- [39] Alejandro Morais Tejerina. 2019. Mapping quantum algorithms in a crossbar architecture.
- [40] Prakash Murali, Dripto M Debroy, Kenneth R Brown, and Margaret Martonosi. 2020. Architecting noisy intermediate-scale trapped ion quantum computers. In *2020 ACM/IEEE 47th Annual International Symposium on Computer Architecture (ISCA)*. IEEE, 529–542.
- [41] Luigi Nardi, David Koeplinger, and Kunle Olukotun. 2019. Practical design space exploration. In *2019 IEEE 27th International Symposium on Modeling, Analysis, and Simulation of Computer and Telecommunication Systems (MASCOTS)*. IEEE, 347–358.
- [42] Shin Nishio, Yulu Pan, Takahiko Satoh, Hideharu Amano, and Rodney Van Meter. 2020. Extracting Success from IBM’s 20-Qubit Machines Using Error-Aware Compilation. *ACM Journal on Emerging Technologies in Computing Systems (JETC)* 16, 3 (2020), 1–25.
- [43] Akito Noiri, Kenta Takeda, Takashi Nakajima, Takashi Kobayashi, Amir Sammak, Giordano Scappucci, and Seigo Tarucha. 2022. Fast universal quantum gate above the fault-tolerance threshold in silicon. *Nature* 601, 7893 (2022), 338–342.
- [44] B Paquelet Wuetz, PL Bavdaz, LA Yeoh, R Schouten, H Van Der Does, M Tiggelman, D Sabbagh, A Sammak, Carmen G Almudever, F Sebastiano, et al. 2020. Multiplexed quantum transport using commercial off-the-shelf CMOS at sub-kelvin temperatures. *npj Quantum Information* 6, 1 (2020), 1–8.
- [45] Nikiforos Paraskevopoulos, Carmen G Almudever, and Sebastian Feld. 2024. beSnake: A routing algorithm for scalable spin-qubit architectures. *IEEE Transactions on Quantum Engineering* (2024).
- [46] Nikiforos Paraskevopoulos, Fabio Sebastiano, Carmen G. Almudever, and Sebastian Feld. 2023. SpinQ: Compilation Strategies for Scalable Spin-Qubit Architectures. *ACM Transactions on Quantum Computing* 5, 1, Article 4 (dec 2023), 36 pages. <https://doi.org/10.1145/3624484>
- [47] SJ Pauka, K Das, R Kalra, A Moini, Y Yang, M Trainer, A Bousquet, C Cantaloube, N Dick, GC Gardner, et al. 2019. A cryogenic interface for controlling many qubits. *arXiv preprint arXiv:1912.01299* (2019).
- [48] Stephan GJ Philips, Mateusz T Madzik, Sergey V Amitonov, Sander L de Snoo, Maximilian Russ, Nima Kalhor, Christian Volk, William IL Lawrie, Delphine Brousse, Larysa Tryputen, et al. 2022. Universal control of a six-qubit quantum processor in silicon. *Nature* 609, 7929 (2022), 919–924.
- [49] Andy D Pimentel. 2022. Methodologies for Design Space Exploration. In *Handbook of Computer Architecture*. Springer, 1–31.
- [50] John Preskill. 2018. Quantum computing in the NISQ era and beyond. *Quantum* 2 (2018), 79.
- [51] Qiskit contributors. 2023. Qiskit: An Open-source Framework for Quantum Computing. <https://doi.org/10.5281/zenodo.2573505>
- [52] Nils Quetschlich, Lukas Burgholzer, and Robert Wille. 2022. Predicting Good Quantum Circuit Compilation Options. *arXiv preprint arXiv:2210.08027* (2022).
- [53] Nils Quetschlich, Lukas Burgholzer, and Robert Wille. 2023. Compiler optimization for quantum computing using reinforcement learning. In *2023 60th ACM/IEEE Design Automation Conference (DAC)*. IEEE, 1–6.
- [54] Saloni Resch and Ulya R Karpuzcu. 2019. Quantum computing: an overview across the system stack. *arXiv preprint arXiv:1905.07240* (2019).
- [55] Marie Salm, Johanna Barzen, Frank Leymann, Benjamin Weder, and Karoline Wild. 2021. Automating the comparison of quantum compilers for quantum circuits. In *Symposium and Summer School on Service-Oriented Computing*. Springer, 64–80.
- [56] Bobak Shahriari, Kevin Swersky, Ziyu Wang, Ryan P Adams, and Nando De Freitas. 2015. Taking the human out of the loop: A review of Bayesian optimization. *Proc. IEEE* 104, 1 (2015), 148–175.
- [57] Ghassan Shobaki, Vahl Scott Gordon, Paul McHugh, Theodore Dubois, and Austin Kerbow. 2022. Register-Pressure-Aware Instruction Scheduling Using Ant Colony Optimization. *ACM Transactions on Architecture and Code Optimization* 19, 2 (6 2022). <https://doi.org/10.1145/3505558>
- [58] Seyon Sivarajah, Silas Dilkes, Alexander Cowtan, Will Simmons, Alec Edgington, and Ross Duncan. 2020. t—ket<sub>q</sub>: a retargetable compiler for NISQ devices. *Quantum Science and Technology* 6, 1 (2020), 014003.
- [59] B. Suman and P. Kumar. 2006. A survey of simulated annealing as a tool for single and multiobjective optimization. , 1143–1160 pages. <https://doi.org/10.1057/palgrave.jors.2602068>
- [60] Brennan Undseth, Xiao Xue, Mohammad Mehmandoust, Maximilian Rimbach-Russ, Pieter T Eendebak, Nodar Samkharadze, Amir Sammak, Viatcheslav V Dobrovitski, Giordano Scappucci, and Lieven MK Vandersypen. 2023. Nonlinear response and crosstalk of electrically driven silicon spin qubits. *Physical Review Applied* 19, 4 (2023), 044078.
- [61] Juan Ungredda and Juergen Branke. 2021. Bayesian Optimisation for Constrained Problems. (5 2021). <http://arxiv.org/abs/2105.13245>
- [62] LMK Vandersypen, H Bluhm, JS Clarke, AS Dzurak, R Ishihara, A Morello, DJ Reilly, LR Schreiber, and M Veldhorst. 2017. Interfacing spin qubits in quantum dots and donors—hot, dense, and coherent. *npj Quantum Information* 3, 1 (2017), 1–10.
- [63] Vlatko Vedral, Adriano Barenco, and Artur Ekert. 1996. Quan-

- tum networks for elementary arithmetic operations. *Physical Review A* 54, 1 (7 1996), 147–153. <https://doi.org/10.1103/PhysRevA.54.147>
- [64] M Veldhorst, HGJ Eenink, Chih-Hwan Yang, and Andrew S Dzurak. 2017. Silicon CMOS architecture for a spin-based quantum computer. *Nature communications* 8, 1 (2017), 1–8.
- [65] Menno Veldhorst, CH Yang, JCC Hwang, W Huang, JP Dehollain, JT Muhonen, S Simmons, A Laucht, FE Hudson, Kohei M Itoh, et al. 2015. A two-qubit logic gate in silicon. *Nature* 526, 7573 (2015), 410–414.
- [66] Chien-An Wang, Valentin John, Hanifa Tidjani, Cécile X Yu, Alexander Ivlev, Corentin Déprez, Floor van Riggelen-Doelman, Benjamin D Woods, Nico W Hendrickx, Will IL Lawrie, et al. 2024. Operating semiconductor quantum processors with hopping spins. *arXiv preprint arXiv:2402.18382* (2024).
- [67] TF Watson, SGJ Philips, Erika Kawakami, DR Ward, Pasquale Scarlino, Menno Veldhorst, DE Savage, MG Lagally, Mark Friesen, SN Coppersmith, et al. 2018. A programmable two-qubit quantum processor in silicon. *nature* 555, 7698 (2018), 633–637.
- [68] Xin-Chuan Wu, Pradnya Khalate, Albert Schmitz, Shavindra Premaratne, Kevin Rasch, Sahar Daraeizadeh, Roza Kotlyar, Shengru Ren, Jennifer Paykin, Francis Rose, et al. 2023. Intel Quantum SDK Version 1.0: Extended C++ Compiler, Runtime and Quantum Hardware Simulators for Hybrid Quantum-Classical Applications. In *APS March Meeting Abstracts*, Vol. 2023. RR08–005.
- [69] Xiao Xue, Maximilian Russ, Nodar Samkharadze, Brennan Undseth, Amir Sammak, Giordano Scappucci, and Lieven MK Vandersypen. 2022. Quantum logic with spin qubits crossing the surface code threshold. *Nature* 601, 7893 (2022), 343–347.
- [70] Jun Yoneda, Kenta Takeda, Tomohiro Otsuka, Takashi Nakajima, Matthieu R Delbecq, Giles Allison, Takumu Honda, Tet-suo Koderu, Shunri Oda, Yusuke Hoshi, et al. 2018. A quantum-dot spin qubit with coherence limited by charge noise and fidelity higher than 99.9%. *Nature nanotechnology* 13, 2 (2018), 102–106.
- [71] DM Zajac, TM Hazard, X Mi, K Wang, and Jason R Petta. 2015. A reconfigurable gate architecture for Si/SiGe quantum dots. *Applied Physics Letters* 106, 22 (2015), 223507.
- [72] Michalewicz Zbigniew. 1996. Genetic algorithms+ data structures= evolution programs. *Computational statistics* 24 (1996), 372–373.
- [73] Floris A. Zwanenburg, Andrew S. Dzurak, Andrea Morello, Michelle Y. Simmons, Lloyd C. L. Hollenberg, Gerhard Klimeck, Sven Rogge, Susan N. Coppersmith, and Mark A. Eriksson. 2013. Silicon quantum electronics. *Rev. Mod. Phys.* 85 (Jul 2013), 961–1019. Issue 3. <https://doi.org/10.1103/RevModPhys.85.961>

## X. APPENDIX

### A. Quantum Circuits

Quantum circuits are defined as a sequence of gates to be executed on qubits (single-qubit gates) or between qubits (two or more qubit gates). Such quantum circuits are often given in a hardware-agnostic description. This means there are no considerations for device-specific restrictions, such as connectivity of qubits or the set of executable gates. Therefore, a compiler [11, 12, 18, 32, 33, 46, 51, 55, 58, 68] is necessary to transform a hardware-agnostic circuit into a circuit that is executable on a given architecture of the device.

We have, therefore, selected a wide range of representative quantum circuits of different qubit counts from Qlib [36] and qbench [2] libraries to thoroughly test SpinQ and ArtA. Tab. VI summarizes all the quantum circuits used in this work.

### B. Optimization Methods

We introduce the five optimization methods, four of which have four different hyper-parameter configurations, totaling seventeen configurations. We will introduce each method, describe the policy it uses to select a new architecture in each iteration of ArtA, give additional details, and finally describe the hyper-parameters used. Some of these methods utilize a distance metric. Given that our analysis primarily involves categorical variables, we will initially discuss our approach to implementing such a distance measure.

#### 1. Distance measure

The notion of distance is hard to apply to values of categorical variables because a categorical variable is defined by having no order between the possible values. For example, the set  $\phi = \{\text{apple, pear, banana}\}$  is categorical, as the “<” sign holds no value when applied to this set. Consequently, no order means no distance can be introduced.

There is only one variable that is categorical: `single_qubit_impl`. To solve this, we postulate an ordering of values by the maximum amount of gates that would be theoretically executed during the same time step. The ordering is then *sequential* < *semi-global* < *local* < *global*, which we will use from now on. This means, for instance, the distance between *sequential* and *semi-global* is 1, but the distance between *sequential* and *local* is 2.

The second challenge is how to combine the distance measured between values of one variable with the distance measured between values of another variable. To describe this, we define  $d$  as the distance between two values of the same variable and  $D$  as the distance between architectures such that the relation between  $D$  and  $d$  is given in Equation 8. This implies that the distance between two architectures is the sum of the distances between the corresponding variable values. Finally, we decided to count all distances in units of 1 and have the

TABLE VI: Summary of all quantum circuits analyzed to answer the third and fourth research questions. All qubit counts, followed by a \*, are used in answering both research questions, while an absence of a symbol indicates algorithms used in the fourth research question only. A ! indicates circuits *only* used in the third research question.

Circuit name	Description	Qubit count
QFT	Produces a highly entangled state including a phase factor [13]	10*, 20*, 40, 50, 60, 100, 150
Grover's search	Used to perform database search [24]	10*, 20*, 50, 80, 90, 100, 150, 200
Quantum Volume	Circuit used for benchmarking quantum computers [14]	8*, 10*, 20, 30, 40
Random circuit	Created to study Quantum Volume behavior	8*!, 10*!
Cuccaro Adder	Used for the addition of two numbers [15]	12*, 22*, 42, 62, 82, 100, 130, 258
vbeAdder	Also used for addition, uses more ancilla qubits [63]	16*, 31*, 61, 91, 121, 148, 193, 385
Bernstein Vazirani	Finds an unknown bitstring [3]	11, 21, 30, 40, 50, 65, 129, 257

distance equal to the difference in indices if we were to order the set of allowed values of one variable. This holds for all values, such that  $d(\text{degree} = 4, \text{degree} = 6) = 1$ ,  $d(\text{degree} = 4, \text{degree} = 8) = 2$ , etc.

$$D(\text{arch}_1, \text{arch}_2) = \sum_{\text{arch\_variable}} d_{\text{arch\_variable}}(\text{arch}_1, \text{arch}_2) \quad (8)$$

## 2. Random Sampling

Random sampling is used as our baseline to compare the optimization methods. It traverses the design space by randomly selecting architectures to investigate. The policy comprises assigning one randomly sampled architecture as the population.

## 3. Simulated Annealing

Simulated annealing (SA) [34] is inspired by the metallurgical process of heating and then slowly cooling a material, which minimizes defects and thus approximates its lowest energy state. SA is a mix of a greedy strategy for selecting the best-performing architecture while trying to escape local optima to find the global optimum. A more detailed overview of simulated annealing can be found in [59]. The policy is as follows:

1. Start with a random architecture, called architecture<sub>*i*</sub>, which has ESP<sub>*i*</sub>, where *i* is the iteration number. It should be noted SA only works with a population size of one, which is the architecture<sub>*i*</sub>.
2. Set a starting temperature  $T_i = T_{\text{start}}$  (hyperparameter set to either 50 or 20).
3. Find a random candidate architecture<sub>*c,i*</sub> which has distance  $D_i$  to architecture<sub>*i*</sub>. We assume that  $D_i$  is randomized but remains greater than 0 to avoid picking the same architecture. Then,  $D_i = \max(\text{Normal}(1, 1) \cdot$

$\text{step\_size}, 1)$ , with  $\text{step\_size}$  used as a hyperparameter equal to either 2 or 3, and  $\text{Normal}(1,1)$  indicates a normal distribution with mean and standard deviation equal to 1. In case no architecture<sub>*c,i*</sub> with distance  $D_i$  to architecture<sub>*i*</sub> is found, a new  $D_i$  is generated, and this step repeats until an architecture<sub>*c,i*</sub> is picked.

4. Calculate the selection probability:  $C_i = \exp((\text{ESP}_{c,i} - \text{ESP}_i)/T_i)$ .
5. Accept the candidate architecture as current architecture if  $C_i > u$ , where  $u$  is a random number between 0 and 1.
6. Update temperature  $T_i$  (cooling process) as  $T_i = (T_{\text{start}}/i)$
7. Repeat steps 3-6 until the TC is met.

The temperature regulates the probability of accepting a candidate architecture with a lower ESP. Specifically, with higher temperatures, there are higher chances of accepting candidate architectures even if they have worse ESP values. However, as temperature decreases, the algorithm only accepts architectures with higher ESP. This mechanism prevents getting stuck in local maxima at the start of the optimization method while gradually becoming greedy at the end by selecting the top-performing architectures only.

## 4. Bayesian Optimization

Bayesian optimization (BO) [22, 56] uses conditional probabilities based on previously sampled data points to predict the function value and uncertainty of subsequently sampled data points. It typically assumes a Gaussian Process (GP) as the statistical model that governs the relation between the function values of points. Our policy for BO is as follows:

- We assume the ESP function has been observed at  $n_o$  architectures at iteration *i*.
- The last  $n_{\text{sample}}$  history (set to 300) of the sampled architectures is selected. We call them  $a_s$ .
- From the unsampled architectures,  $n_{\text{candidate}}$  amount (set to

1000) architectures are selected. We call them  $a_c$ .

- $a_s$  is used to build a surrogate function for  $a_c$ . The surrogate function predicts the mean and standard deviation for each architecture in  $a_c$ . This surrogate function is constructed with a *mean function*  $\mu_0$  and a covariance matrix by evaluating a *kernel*  $\Sigma_0$ .
- Given the surrogate function, we compute the acquisition function. This acquisition function uses each architecture's mean and standard deviation in  $a_c$  to determine whether an architecture should be evaluated. It balances a high expected value (exploitation) with a high uncertainty (exploration). As explained later, there are many acquisition functions, each with its own approach to making this exploitation/exploration trade-off.
- From  $a_c$  we choose  $n_{\text{size pop}}$  (set to 50) architectures, namely those with the highest value of the acquisition function.

For discrete functions in the BO algorithm, all non-integer valued points are first rounded to integers before calculating their expected value [23]. Additionally, since not all combinations of architecture variables constitute valid architectures, we use a BO formulation for constrained problems [61]. Therefore, we only sample from valid architectures, which automatically satisfy the constraints and only contain the integer values for variables that are of interest to our problem.

For each architecture  $a \in a_c$ , our GP assumption lets us compute the conditional distribution of ESP using Bayes' rule [21].

$$\text{ESP}(a)|\text{ESP}(a_s) \sim \text{Normal}(\mu_s(a), \sigma_s^2(a)) \quad (9)$$

where,

$$\mu_s(a) = \Sigma_0(a, a_s)\Sigma_0(a_s, a_s)^{-1}(\text{ESP}(a_s) - \mu_0(a_s)) + \mu_0(a) \quad (10)$$

and,

$$\sigma_s^2(a) = \Sigma_0(a, a) - \Sigma_0(a, a_s)\Sigma_0(a_s, a_s)^{-1}\Sigma_0(a_s, a) \quad (11)$$

For the mean function, we use the arithmetic mean as:

$$\mu_0(x)|a_s = \frac{1}{s} \sum_{i=1}^s (\text{ESP}_i) \quad (12)$$

Two different Kernels are used, namely the Gaussian Kernel and the Matérn Kernel [21] with  $\nu = 1.5$ , both of which are commonly used for BO problems. They are defined as follows:

$$\Sigma_0(a_a, a_b) = \begin{cases} \text{Gaussian} \\ \exp(-\|a_a - a_b\|^2) \\ \text{Matérn} \\ (1 + \sqrt{3}\|a_a - a_b\|) \cdot \exp(-\sqrt{3}\|a_a - a_b\|) \end{cases} \quad (13)$$

Given this surrogate function, an acquisition function (AF) is calculated to determine which points will be sampled next. To this end, we use Expected Improvement (EI) and Upper

Confidence Bound (UCB) as AF, defined as:

$$\text{AF}(a) = \begin{cases} \text{EI:} \\ (\mu_s(a) - \max(\text{ESP}_s)) \cdot \text{CDF}(Z) + \sigma_s(a) \cdot \text{PDF}(Z) \\ \text{UCB:} \\ \mu_s(a) + \sigma_s(a) \end{cases} \quad (14)$$

With  $Z = (\mu_s(a) - \max(\text{ESP}_s))/(\sigma_s(a))$ . CDF and PDF are the Cumulative/Probability Density Functions, respectively. Variable  $\max(\text{ESP}_s)$  equals the highest ESP value found for all architectures present in  $a_s$ . ArtA then picks the new architectures with the highest acquisition function values to sample in the new iteration until the TC is met.

## 5. Genetic Algorithm

Genetic algorithm (GA) [72] is modeled after the biological evolution of genes to arrive at a near-optimal solution for an optimization problem. The GA changes the architectural variables of high-performing architectures to explore and discover even better-performing architectures with the use of three operations: selection, mutation, and cross-over. The GA policy works as follows:

- Every generation's iteration,  $i$ , considers a population of size  $n$  (hyperparameter set to either 50 or 100). The population at generation  $i + 1$  consists of elite, cross-over, and mutation children. These are explained next.
- From these  $n$  architectures,  $n_{\text{elite}}$  individuals (set to 15% of  $n$ ) with the highest ESP value are selected and automatically included in our population of the next generation.
- Additionally,  $n_{\text{parent}}$  (set to 50% of  $n$ ) out of  $n$  architectures are selected iteratively by randomly considering  $n_{\text{tournament}}$  architectures (set to 5) from the population and selecting the one with the highest ESP value. There are no duplicate parents.
- Two parents of this group are selected randomly. Cross-over is performed by picking a random cross-over point  $c$  with  $1 \leq c \leq k$ , where  $k$  is the total number of architectural variables of the design space. A new architecture is formed by combining the architectural variables of the two parents, with  $c$  indicating the index separating the two halves of the variable list. The process is repeated if this is not a valid architecture.  $n_{\text{cross-over}}$  (set to 30% of  $n$ ) architectures are created in this way.
- The remaining new generation is populated with  $n_{\text{mut}}$  architectures (set to 55% of  $n$ ). For this operation, some children (from before) alter each of their architectural variable values with probability  $p_{\text{mut}}$  (hyperparameter set to either 0.15 or 0.2). The process is repeated if this is not a valid architecture.
- The algorithm repeats until the TC is met.

Note that in GA (as in SA), it is possible to have the same architecture in multiple populations.

